CrossMark

ORIGINAL ARTICLE

Performance characteristics of a novel clustered multi-pinhole technology for simultaneous high-resolution SPECT/PET

Kenta Miwa[1,2,3] · Masayuki Inubushi[4] · Yasuto Takeuchi[1] · Tetsuro Katafuchi[5] · Mitsuru Koizumi[1,2] · Tsuneo Saga[1] · Masayuki Sasaki[3]

Abstract

Objective Versatile emission computed tomography (VECTor) for small-animal imaging enables fully simultaneous SPECT/PET image acquisition based on clustered multi-pinhole collimation. The present study experimentally evaluated the detailed performance characteristics of the clustered multi-pinhole system for simultaneous ^{99m}Tc and ^{18}F imaging from the user perspective.

Methods Spatial resolution, sensitivity, count rate linearity were determined for the VECTor system (MILabs). Two hot-rod micro-resolution phantoms with 6 sectors were created to test the resolution of ^{99m}Tc and ^{18}F. Sensitivity and count rate linearity were measured by scanning ^{99m}Tc and ^{18}F point sources positioned at the center of the field of view. Furthermore, we quantified the influence of ^{18}F on ^{99m}Tc SPECT images. The ratios of SPECT counts on the ^{99m}Tc-only and simultaneous ^{18}F-^{99m}Tc at various time points were evaluated as a function of the ^{18}F-to-^{99m}Tc activity concentration ratio.

Results The 0.5-mm hot-rods can be visually distinguished in the ^{99m}Tc image, and 0.8-mm rods for ^{18}F remained clearly visible. The point-source sensitivity was 2800 cps/MBq for ^{99m}Tc and 2899 cps/MBq for ^{18}F, respectively. Count rates up to 120,000 cps for one bed position were linear for the activity. Spill-over from ^{18}F into ^{99m}Tc SPECT images was negligible when the activity concentration of the administered ^{18}F solution exceeded that of the ^{99m}Tc solution by up to a factor of 2.

Conclusions We evaluated the performance characteristics of the VECTor that lead to determination of the optimal administered doses of ^{99m}Tc and ^{18}F tracers. We found that the VECTor achieved high resolution and high sensitivity as well as good ^{99m}Tc and ^{18}F linearity. Simultaneous SPECT/PET imaging with ^{99m}Tc and ^{18}F tracers, and stand-alone ^{99m}Tc and ^{18}F imaging using clustered-pinhole collimators is feasible and practical for a wide range of research applications using small animals.

Keywords VECTor · Simultaneous imaging · Clustered multi-pinhole · Small-animal imaging · SPECT/PET

K. Miwa and M. Inubushi contributed equally.

✉ Masayuki Inubushi
  inubushi@med.kawasaki-m.ac.jp

  Kenta Miwa
  kenta5710@gmail.com

[1] Molecular Imaging Center, National Institute of Radiological Sciences, 4-9-1 Anagawa, Inage-ku, Chiba-shi, Chiba 263-8555, Japan

[2] Department of Nuclear Medicine, Cancer Institute Hospital of Japanese Foundation for Cancer Research, 3-8-31 Ariake, Koto-ku, Tokyo 135-8550, Japan

[3] Division of Medical Quantum Science, Department of Health Sciences, Graduate School of Medical Sciences, Kyushu University, 3-1-1 Maidashi, Higashi-ku, Fukuoka 812-8582, Japan

[4] Division of Nuclear Medicine, Department of Radiology, Kawasaki Medical School, 577 Matsushima Kurashiki, Okayama 701-0192, Japan

[5] Department of Radiological Technology, Gifu University of Medical Science, 795-1 Nagamine, Ichihiraga, Seki-shi, Gifu 501-3892, Japan

Introduction

Molecular imaging of small animals with single photon emission tomography (SPECT) and positron emission tomography (PET) has recently emerged as an important tool with which to assess molecular mechanisms and

Springer

pharmaceutical development [1]. Sub-half-millimeter (mm) SPECT resolution is useful for systems equipped with multi-pinhole collimators [2, 3], but sub-mm resolution has recently been achieved for PET tracers using pinholes [4]. SPECT and PET play complementary roles in multimodality imaging [5, 6]. Thus, the simultaneous SPECT and PET imaging might gain new insight into the multiple biologic mechanisms by visualizing and quantifying different aspects of biologic function.

Multimodality preclinical imaging systems have recently been integrated into a common gantry and are now commercially available [7]. Examples of such preclinical trimodality systems are the versatile emission computed tomography/computed tomography (VECTor/CT) [8, 9], Triumph[TM] Trimodality System [10], Inveon PET/SPECT/CT [5] and ALBIRA [11, 12]. Although the Triumph, Inveon and ALBIRA systems cannot simultaneously acquire SPECT and PET images, VECTor enables fully simultaneous SPECT/PET image acquisition based on clustered-pinhole collimation [8].

Pinhole edge penetration by 511 keV annihilation photons renders current multi-pinhole collimators unsuitable for the high-resolution imaging of positron emitters [4]. Although reducing pinhole acceptance angles can reduce resolution loss due to edge penetration, such improvement is achieved at the cost of each pinhole having a reduced field of view (FOV). Goorden et al. [4, 13] developed a novel collimation system using clustered pinholes to simultaneously and separately image γ-photons emitted by PET and SPECT tracers. The central FOV in this clustered multi-pinhole system is kept equal to that of the conventional pinhole system by selecting an opening angle of 16° and 18° for each pinhole in the cluster [8].

The manufacturers have recently published information about the basic performance of the VECTor system [8]. Although they have proven that the image quality in terms of resolution, contrast, and the count-to-noise ratio is superior to conventional PET system [9], the detailed performance under several different conditions has not been evaluated yet. The present study experimentally evaluates the performance of the clustered multi-pinhole system for simultaneous ^{99m}Tc and ^{18}F imaging from the user perspective.

Materials and methods

System and collimator geometry

The VECTor system (MILabs, Utrecht, Netherlands) designed for simultaneous SPECT and PET imaging of small animals. This system comprises three stationary gamma detectors in a triangular configuration. The NaI(Tl) crystals have an active area of 51×38 mm^2 and a thickness of 9.5 mm. The exchangeable cylindrical clustered-pinhole collimators are placed in the center of the system. The clustered-pinhole collimator designed for high-energy photons (511 keV) is previously described [4]. The clustered-pinhole collimator made of tungsten contains 48 clusters of four 0.7-mm-diameter pinholes placed in four rings (Fig. 1a, b). Of 192 clustered pinholes, 162 were used for image reconstruction. The collimator has a wall thickness of 43 mm, an inner diameter of 48 mm and the pinhole centers are placed at a diameter of 64 mm. The diameter of the central FOV in the clustered-pinhole collimator described herein was 12 mm and the longitudinal length was 9 mm.

Data acquisition and image reconstruction

Data were acquired using the scanning focus method as proposed by Vastenhouw and Beekman [14]. The photopeak windows of all SPECT and PET data in this study were set to a width of 20 %. Images were reconstructed using a pixel-based ordered-subsets expectation maximization (POSEM) algorithm with 16 subsets and 10 iterations. All SPECT and PET images were reconstructed on a 0.4 mm voxel grid with MILabs reconstruction software (β version).

Scatter correction used a triple-energy-window (TEW) technique [15] and was performed on the all SPECT and PET data. The background windows were set to 100–115 and 155–170 keV for ^{99m}Tc tracers and 400–450 and 550–600 keV for ^{18}F tracers. No attenuation correction was applied.

Evaluation of system characteristics

Spatial resolution and sensitivity of stand-alone ^{99m}Tc and ^{18}F imaging

Two hot-rod micro-spatial resolution phantoms with 6 sectors were created to test the resolution. The capillary diameters were 0.35, 0.40, 0.45, 0.50, 0.60 and 0.75 mm, in the phantom containing ^{99m}Tc and 0.45, 0.5, 0.55, 0.75, 0.8 and 0.85 mm in the phantom containing ^{18}F. The capillaries contained 40 MBq of ^{99m}Tc and 44 MBq of ^{18}F at the start of scanning.

Sensitivity was measured by scanning ^{99m}Tc and ^{18}F point sources with 15 MBq activity positioned at the center of the FOV. The acquisition time was 10 min. Sensitivity was calculated by dividing the counts in the photopeak by the measured activity using Eq. 1:

$$\text{Sensitivity}\left(^{\text{cps}}/_{\text{MBq}}\right) = \frac{\text{Count}-\text{rate in photopeak}}{A_{t0}} \qquad (1)$$

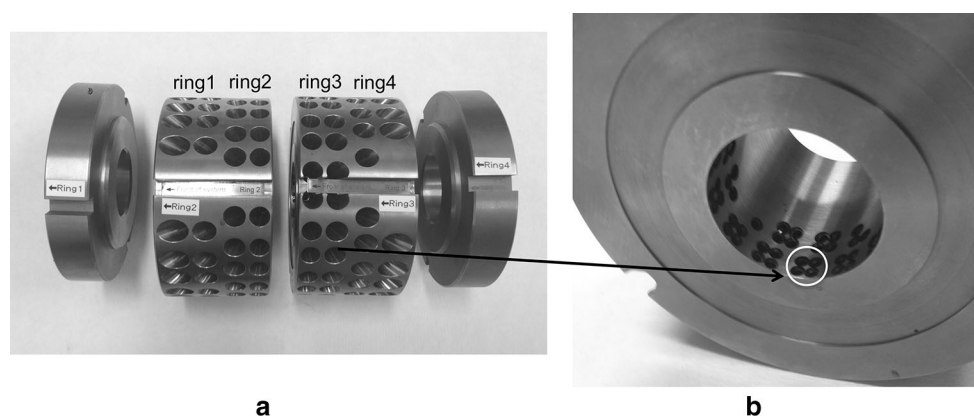where A_{t0} represents the measured activity.

Fig. 1 Clustered-pinhole collimator optimized for imaging SPECT and PET tracers. **a** The collimator of tungsten comprising four rings. **b** Clusters of four 0.7-mm-diameter pinholes (*white circle*). The collimator contains 48 clusters placed in four rings (*inner view*)

Count rate linearity

Count rate as a function of activity was measured using a point-source phantom comprising a 0.2-mL micro-tube. A phantom with a volume 0.1 mL containing either <800 MBq of ^{99m}Tc or 418 MBq of ^{18}F was positioned along the axis of the scanner and centered in the FOV. The phantom was fully covered by the 3-dimensional central FOV (an ellipsoid of $12 \times 12 \times 9$ mm).

Nine phantoms contained 3, 6, 12, 25, 50, 100, 200, 400 and 800 MBq of a homogeneous ^{99m}Tc solution. The photopeak counts at each time frame with a 30-min acquisition period were calculated to determine count rates.

We used the decay method to generate count response curves for an initially high ^{18}F activity concentration that was allowed to decay. List-mode acquisition proceeded for 20 h (11 half-lives of ^{18}F) until the activity decayed to <0.2 MBq. Each 30-min section of list-mode data was binned and the photopeak counts were recorded.

The count rate linearity performances of ^{99m}Tc and ^{18}F were evaluated by the relationship between the measured count rates and the activity.

Spill-over of ^{18}F into ^{99m}Tc SPECT images

We quantified the influence of ^{18}F on ^{99m}Tc SPECT images as follows. One point-source phantom with a volume of 0.1 mL was filled with a mixture of ^{99m}Tc (37 MBq) and ^{18}F (370 MBq). The other was filled with only the ^{99m}Tc (37 MBq). The phantom was fully covered by the central FOV. List-mode acquisition proceeded for 12 h/scan. The SPECT images were reconstructed from the list-mode data. The region of interest (ROI) covering the entire phantom in the projection was used for SPECT. The photopeak counts at each time frame with a 30-min acquisition period were calculated. Ratios of SPECT counts on the ^{99m}Tc-only and

simultaneous ^{18}F-^{99m}Tc at various time points ($t = 0$, 1 and 2–12 h) were evaluated as a function of the ^{18}F-to-^{99m}Tc radioactivity concentration ratio.

Results

Figure 2 shows representative images of the spatial resolution phantom containing ^{99m}Tc and ^{18}F tracers. The 0.5-mm hot-rods can be visually distinguished in the ^{99m}Tc image, and 0.8-mm rods for ^{18}F are visible. The sensitivity measured with ^{99m}Tc and ^{18}F was 2800 cps/MBq (0.28 %) for ^{99m}Tc and 2899 cps/MBq (0.29 %) for ^{18}F, respectively.

Figure 3 shows count rates as a function of activity of ^{99m}Tc and ^{18}F. The peak count rates of ^{99m}Tc and ^{18}F were 588 kcps at 427 MBq and 264 kcps at 196 MBq,
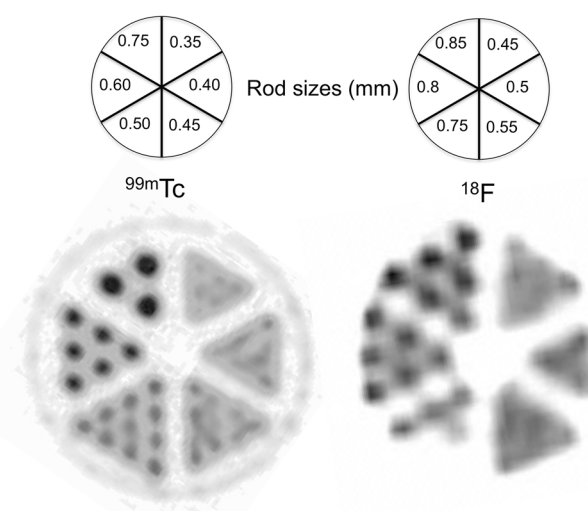

Fig. 2 Reconstructed images of ^{99m}Tc and ^{18}F in thin hot-rod phantoms. Slice thickness is 0.4 mm
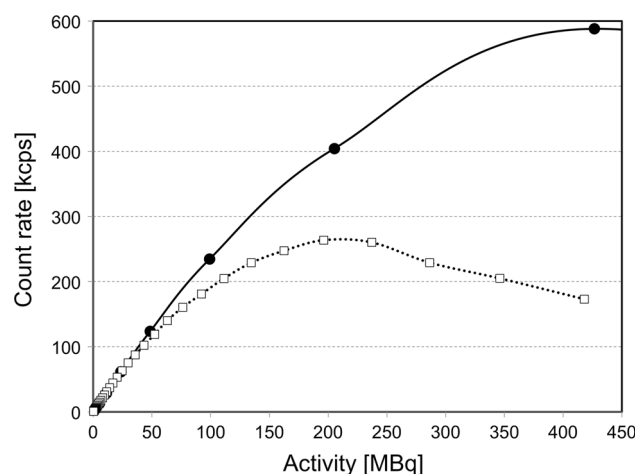
Fig. 3 Count rates as a function of activity of ^{99m}Tc and ^{18}F using 0.1-mL point source. *Circle* ^{99m}Tc, *square* ^{18}F

respectively. The slope of the resulting linearity curve for ^{99m}Tc was roughly equal to that for ^{18}F at low activity up to 50 MBq, whereas at high activity levels the count rate of ^{18}F was limited.

Figure 4 shows the energy spectra of the ^{99m}Tc, ^{18}F and simultaneous ^{99m}Tc and ^{18}F images. The ^{99m}Tc-imaging spectrum showed only the 141-keV photopeak for ^{99m}Tc (Fig. 4a), whereas ^{18}F-imaging spectrum showed that energy spectra except for the primary photopeak were measured at 170 keV in the photopeak windows (Fig. 4b). In simultaneous ^{99m}Tc and ^{18}F images, three events at 141, 170 and 511 keV were measured (Fig. 4c). The energy spectrum of ^{99m}Tc was slightly distorted due to the close proximity of the photopeaks of 141 and 170 keV.

Figure 5 shows SPECT count ratios of ^{99m}Tc-alone and ^{18}F-^{99m}Tc simultaneous SPECT in relation to the
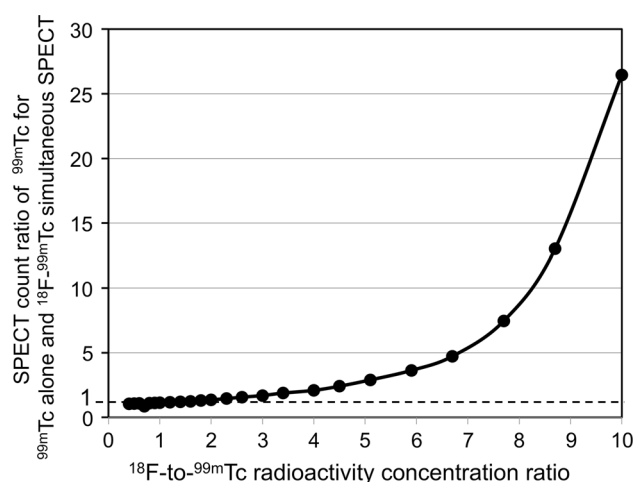

Fig. 5 The SPECT count ratio of ^{99m}Tc for ^{99m}Tc-alone and ^{18}F-^{99m}Tc simultaneous acquisition in relation to ^{18}F-to-^{99m}Tc radioactivity concentration ratio. For the data, TEW scatter correction was employed

^{18}F-to-^{99m}Tc radioactivity concentration ratio. The SPECT count ratio of ^{99m}Tc in stand-alone to ^{99m}Tc in simultaneous images remained constant (almost 1) up to an ^{18}F:^{99m}Tc concentration ratio of 2:1. It exponentially increased with an increase of ^{18}F-to-^{99m}Tc radioactivity ratio.

Discussion

We evaluated the performance characteristics and imaging capability of a contemporary high-tech SPECT/PET/CT system for imaging small animals. The manufacturers have recently published information about the basic performance of the VECTor system [8, 9]. However, the present
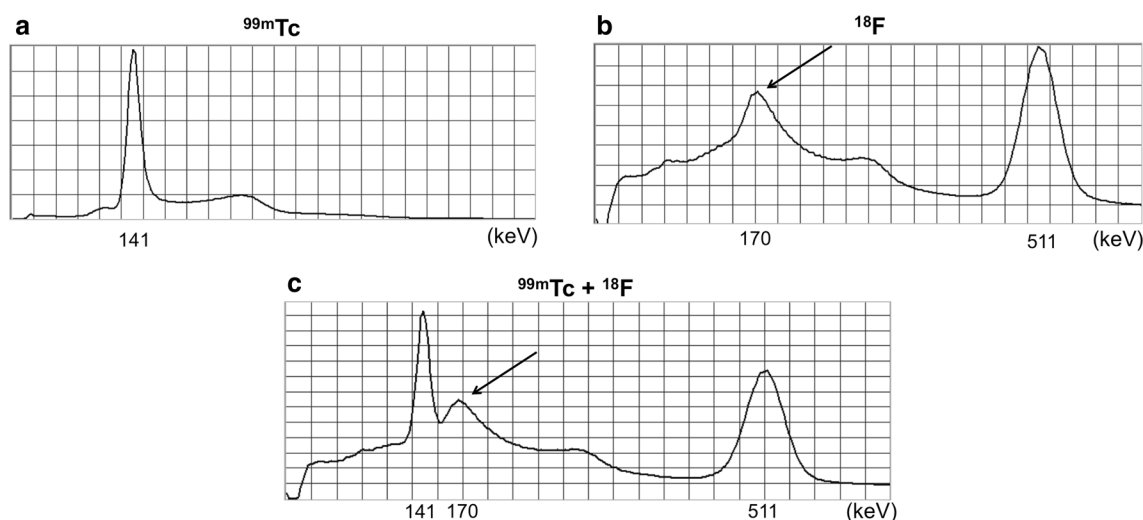

Fig. 4 Spectra with clustered-pinhole collimator in stand-alone ^{99m}Tc (**a**) and ^{18}F (**b**) images and in simultaneous ^{99m}Tc and ^{18}F image (**c**). The activities for ^{99m}Tc and ^{18}F were about 37 and 370 MBq, respectively. *Black arrow* photopeak of 170 keV originated from ^{18}F at high photopeak energy

study assessed detailed performance characteristics that lead to determination of the optimal administered doses of ^{99m}Tc and ^{18}F tracers. The VECTor system achieved high resolution and high sensitivity as well as good ^{99m}Tc and ^{18}F linearity.

Visual assessment using a spatial resolution phantom instead of the full width at half maximum (FWHM) of a line phantom is likely to provide spatial resolution estimates closer to the actual values obtained during small-animal imaging studies [16]. In our scanner, an imaging study using two types of phantoms resolved 0.5- and 0.8-mm rods for ^{99m}Tc and ^{18}F tracers, respectively, showing the actual sub-mm imaging capability of the VECTor system. Previous reports have indicated that spatial resolution for ^{99m}Tc SPECT of Triumph [10], Inveon [5] and ALBIRA [11, 12] are 0.4, 1 and 0.8 mm, respectively, and 1.35, 1.4 and 1.55 mm for ^{18}F PET, respectively. Thus, our results of VECTor were better than that of previously developed devices [11, 17]. Goorden et al. [4] showed that clustered pinholes could offer improved spatial resolution. In addition, our results of stand-alone imaging corresponded to those of previous studies of simultaneous imaging [8]. We consider that the quality of simultaneous ^{99m}Tc and ^{18}F images acquired using the VECTor can compete with that of individual ^{99m}Tc and ^{18}F images. In general, SPECT has better spatial resolution, whereas PET is more sensitive when imaging small animals. The sensitivity was relatively lower for pinhole, than coincidence PET with Triumph, Inveon and ALBIRA (peak sensitivity: 0.29 vs. 6 %, 6.7 and 2 %, respectively). Nevertheless, we acquired high-resolution PET images that compared favorably with the Triumph, Inveon and ALBIRA PET systems. In fact, most dedicated small-animal SPECT/PET systems use pinhole collimation for the most optimal resolution–sensitivity trade-off [18, 19].

A small-animal SPECT/PET system should be able to handle a wide range of count rates without serious losses in count rate linearity. The count rate performance of ^{99m}Tc and ^{18}F tracers with clustered-pinhole collimators has not been evaluated until now. Count rate curves might considerably vary depending on the phantom [20, 21]. We adopted a 0.1-mL point source, which be fully covered over one bed position and the size is similar to that of a mouse organ (12-mm diameter). The slope of the resulting linearity curve for ^{99m}Tc was essentially equal to that of ^{18}F, as count rates for both were linear up to an activity of 50 MBq (~120,000 cps), as seen in Fig. 3. These results indicate that the quantitative performance of the VECTor system at activity levels used in most biologic SPECT or PET experiments is excellent. Harteveld et al. [22] have shown that count loss in terms of U-SPECT-II (VECTor without the clustered-pinhole collimator) performance is not so important in view of the highly linear relationship

between count rate and source activity. However, resolution might deteriorate at high-count rates due to event pile-up [23, 24]. The VECTor system could handle events in ^{99m}Tc and ^{18}F solutions with maximum count rates of 600,000 and 250,000 cps, respectively. Systematic difference in count rate curves could be explained by count loss due to crystal thickness. The VECTor has γ-detectors [NaI(Tl) crystal thickness, 9.5 mm] that are optimized for imaging SPECT tracers. NaI(Tl) crystal is not ideal for positron imaging due to its inherent low efficiency for stopping photons. The NaI(Tl) crystal of the VECTor is 9.5 mm thick, which means that only about 10 % of the 511-keV γ-photons that reach the detector are detected in the photopeak [13].

Clustered pinholes with smaller acceptance angles than traditional pinholes will normally reduce photon penetration [4, 13]. Goorden et al. [13] performed Monte Carlo simulations to quantitatively evaluate the effect of scattered and penetrating photons, and thus indicated that photon scatter from clustered-pinhole collimators was negligible. However, when ^{18}F imaging, energy spectra except for the primary photopeak were measured at 170 keV in the photopeak windows. We consider that the spectrum is mainly due to the backscatter of photons interacting with the clustered-pinhole collimator of tungsten. This is confirmed by the existence of Compton edge of approximately 340 keV (Fig. 4) [25]. In simultaneous ^{99m}Tc and ^{18}F imaging, the image reconstructed with the counts of primary photons emitted from ^{99m}Tc with low photopeak energy is distorted by backscatter photons that originated from ^{18}F at high photopeak energy. Thus, such photons might influence quantitative and imaging data when dealing with high-activity [18]F.

Activities are typically higher in SPECT than in PET studies [26]. However, studies using VECTor require higher doses of PET tracer because the pinhole PET has only one-tenth of the sensitivity of coincidence PET. Thus, some PET tracer might induce spill-over into SPECT images. The limits of equipment performance that can compensate for spill-over must be identified. The ratio of stand-alone to simultaneous SPECT imaging is theoretically constant. However, spill-over from ^{18}F into the ^{99m}Tc images would affect this ratio, resulting in an increased ratio of stand-alone to simultaneous SPECT imaging counts when the ^{18}F-to-^{99m}Tc concentration ratio is >2. Correction for increasing down scatter from ^{18}F with increasing activity ratio can potentially adversely affect the noise and resolution in the ^{99m}Tc image. It has been shown that for ratios <2.9 [8], this effect is very minor and can be tolerated. In this study, we adopted the activities of 37 MBq for ^{99m}Tc that typically used in most biologic SPECT experiments [8]. Since the count losses of ^{99m}Tc and ^{18}F induced by dead time losses are different as shown in

Fig. 3, the starting ^{99m}Tc activity might have influenced the results of the acceptable the ^{18}F-to-^{99m}Tc concentration ratio. Further studies of spill-over with various combined sources are required.

The presence of large backscatter photopeak (170 keV gamma photons) causes errors in scatter correction based on the TEW method. Although the TEW method provides a reasonable correction for scatter [27], the similarity between the 141 keV primary and 170 keV backscatter of ^{18}F energy spectra causes difficulties with compensating for scatter events using techniques that are based on spectral analysis [28]. We do not consider it enough to use only the conventional TEW method for the scatter correction including backscatter of VECTor. Further study is warranted to elucidate the compensation for 170 keV backscatter on simultaneous ^{99m}Tc/^{18}F experiments.

The present study is limited by the fact that all images acquired using ^{99m}Tc and ^{18}F solutions were reconstructed under identical conditions. Reconstruction parameters should be carefully selected according to the experimental objectives and tracers because image quality considerably varies depending on the selected values [29]. This trade-off between the recovery of small structures and image noise influenced by the number of iterations and spatial filtering should be considered in the reconstruction setting [30].

Conclusions

We evaluated the performance characteristics and imaging capability of the VECTor system from the user perspective and found that the resolution and sensitivity of ^{99m}Tc and ^{18}F imaging is high. Count rates up to 120,000 cps for one bed position were linear for activity, indicating excellent quantitative performance. Spill-over from ^{18}F into ^{99m}Tc SPECT images was negligible when the activity concentration of the administered ^{18}F solution exceeded that of the ^{99m}Tc solution by up to a factor of 2. Simultaneous ^{99m}Tc SPECT/^{18}F PET imaging with two nuclides as well as stand-alone ^{99m}Tc and ^{18}F imaging using clustered-pinhole collimators is feasible and practical for a wide range of research applications using small animals.

Conflict of interest The authors declare that they have no conflict of interest.

References

1. de Kemp RA, Epstein FH, Catana C, Tsui BM, Ritman EL. Small-animal molecular imaging methods. J Nucl Med. 2010;51(Suppl):18–32.
2. Umeda IO, Tani K, Tsuda K, Kobayashi M, Ogata M, Kimura S, et al. High resolution SPECT imaging for visualization of intra-tumoral heterogeneity using a SPECT/CT scanner dedicated for small animal imaging. Ann Nucl Med. 2012;26(1):67–76.
3. Higaki Y, Kobayashi M, Uehara T, Hanaoka H, Arano Y, Kawai K. Appropriate collimators in a small animal SPECT scanner with CZT detector. Ann Nucl Med. 2013;27(3):271–8.
4. Goorden MC, Beekman FJ. High-resolution tomography of positron emitters with clustered pinhole SPECT. Phys Med Biol. 2010;55(5):1265–77.
5. Magota K, Kubo N, Kuge Y, Nishijima K, Zhao S, Tamaki N. Performance characterization of the Inveon preclinical small-animal PET/SPECT/CT system for multimodality imaging. Eur J Nucl Med Mol Imaging. 2011;38(4):742–52.
6. Visser EP, Disselhorst JA, Brom M, Laverman P, Gotthardt M, Oyen WJ, et al. Spatial resolution and sensitivity of the Inveon small-animal PET scanner. J Nucl Med. 2009;50(1):139–47.
7. Koba W, Jelicks LA, Fine EJ. MicroPET/SPECT/CT imaging of small animal models of disease. Am J Pathol. 2013;182(2):319–24.
8. Goorden MC, van der Have F, Kreuger R, Ramakers RM, Vastenhouw B, Burbach JP, et al. VECTor: a preclinical imaging system for simultaneous submillimeter SPECT and PET. J Nucl Med. 2013;54(2):306–12.
9. Walker MD, Goorden MC, Dinelle K, Ramakers RM, Blinder S, Shirmohammad M, et al. Performance assessment of a preclinical PET scanner with pinhole collimation by comparison to a coincidence-based small-animal PET scanner. J Nucl Med. 2014;55(8):1368–74.
10. Prasad R, Ratib O, Zaidi H. NEMA NU-04-based performance characteristics of the LabPET-8^{TM} small animal PET scanner. Phys Med Biol. 2011;56(20):6649–64.
11. Sánchez F, Orero A, Soriano A, Correcher C, Conde P, González A, et al. ALBIRA: a small animal PET/SPECT/CT imaging system. Med Phys. 2013;40(5):051906.
12. Spinks TJ, Karia D, Leach MO, Flux G. Quantitative PET and SPECT performance characteristics of the Albira Trimodal preclinical tomograph. Phys Med Biol. 2014;59(3):715–31.
13. Goorden MC, van der Have F, Kreuger R, Beekman FJ. An efficient simulator for pinhole imaging of PET isotopes. Phys Med Biol. 2011;56(6):1617–34.
14. Vastenhouw B, Beekman F. Submillimeter total-body murine imaging with U-SPECT-I. J Nucl Med. 2007;48(3):487–93.
15. Ogawa K, Harata Y, Ichihara T, Kubo A, Hashimoto S. A practical method for position-dependent Compton-scatter correction in single photon emission CT. IEEE Trans Med Imaging. 1991;10(3):408–12.
16. Boisson F, Zahra D, Parmar A, Gregoire MC, Meikle SR, Hamse H, et al. Imaging capabilities of the inveon SPECT system using single-and multipinhole collimators. J Nucl Med. 2013;54(10):1833–40.
17. Deleye S, Van Holen R, Verhaeghe J, Vandenberghe S, Stroobants S, Staelens S. Performance evaluation of small-animal multipinhole μSPECT scanners for mouse imaging. Eur J Nucl Med Mol Imaging. 2013;40(5):744–58.
18. van der Have F, Vastenhouw B, Ramakers RM, Branderhorst W, Krah JO, Ji C, et al. U-SPECT-II: an ultra-high-resolution device for molecular small-animal imaging. J Nucl Med. 2009;50(4):599–605.

19. Branderhorst W, Vastenhouw B, van der Have F, Blezer EL, Bleeker WK, Beekman FJ. Targeted multi-pinhole SPECT. Eur J Nucl Med Mol Imaging. 2011;38(3):552–61.

20. Sanchez F, Moliner L, Correcher C, Gonzalez A, Orero A, Carles M, et al. Small animal PET scanner based on monolithic LYSO crystals: performance evaluation. Med Phys. 2012;39(2):643–53.

21. Schäfers KP, Reader AJ, Kriens M, Knoess C, Schober O, Schäfers M. Performance evaluation of the 32-module quadHIDAC small-animal PET scanner. J Nucl Med. 2005;46(6): 996–1004.

22. Harteveld AA, Meeuwis AP, Disselhorst JA, Slump CH, Oyen WJ, Boerman OC, et al. Using the NEMA NU 4 PET image quality phantom in multipinhole small-animal SPECT. J Nucl Med. 2011;52(10):1646–53.

23. Nagy K, Tóth M, Major P, Patay G, Egri G, Häggkvist J, et al. Performance evaluation of the small-animal nanoScan PET/MRI system. J Nucl Med. 2013;54(10):1825–32.

24. Wang Y, Seidel J, Tsui BM, Vaquero JJ, Pomper MG. Performance evaluation of the GE healthcare eXplore VISTA dual-ring small-animal PET scanner. J Nucl Med. 2006;47(11):1891–900.

25. Spanoudaki VC, Lau FW, Vandenbroucke A, Levin CS. Physical effects of mechanical design parameters on photon sensitivity and spatial resolution performance of a breast-dedicated PET system. Med Phys. 2010;37(11):5838–49.

26. Funk T, Sun M, Hasegawa BH. Radiation dose estimate in small animal SPECT and PET. Med Phys. 2004;31(9):2680–6.

27. Wu C, van der Have F, Vastenhouw B, Dierckx RA, Paans AM, Beekman FJ. Absolute quantitative total-body small-animal SPECT with focusing pinholes. Eur J Nucl Med Mol Imaging. 2010;37(11):2127–35.

28. Dewaraja YK, Ljungberg M, Koral KF. Characterization of scatter and penetration using Monte Carlo simulation in 131I imaging. J Nucl Med. 2000;41(1):123–30.

29. Disselhorst JA, Brom M, Laverman P, Slump CH, Boerman OC, Oyen WJ, et al. Image-quality assessment for several positron emitters using the NEMA NU 4-2008 standards in the Siemens Inveon small-animal PET scanner. J Nucl Med. 2010;51(4): 610–7.

30. Visser EP, Disselhorst JA, Lier MGTB, Laverman P, de Jong GM, Oyen WJG, et al. Characterization and optimization of image quality as a function of reconstruction algorithms and parameter settings in a Siemens Inveon small-animal PET scanner using the NEMA NU4-2008 standards. Nucl Instrum Methods Phys Res A. 2011;629:357–67.